

DOI: 10.1002/adem.201300405

## ZnSe-Based Longitudinal Twinning Nanowires\*\*

By Jing Xu, Aijiang Lu, Chunrui Wang,\* Rujia Zou, Xiaoyun Liu, Xing Wu, Yuxi Wang, Sijia Li, Litao Sun,\* Xiaoshuang Chen,\* Hongseok Oh, Hyeonjun Baek, Gyu-Chul Yi\* and Junhao Chu

*Zinc blende ZnSe longitudinal twinning nanowires and a sandwich structure with the wurtzite ZnSe inserting into the zinc blende ZnSe longitudinal twinning nanowires are fabricated via a simple thermal evaporation method. The high-resolution transmission electron microscope images of the two types of nanowires match well with simulated atomic models of them. The growth of them might be caused by the crystal plane slip during the phase transformation process between the wurtzite and the zinc blende ZnSe nanowire. The vibrating and luminescence properties of the as-grown longitudinal twinning nanowire are investigated by room-temperature Raman and low-temperature (10 K) photoluminescence spectroscopy, respectively. The electrical transport properties of the two types of longitudinal twinning ZnSe nanowires and the monocrystal ZnSe nanowires were compared using in situ measurement in transmission electron microscope.*

[\*] Prof. C. Wang, J. Xu, Dr. A. Lu, Dr. X. Liu, Dr. R. Zou  
Prof. X. Chen, Prof. J. Chu  
Department of Applied Physics and State Key Laboratory for Modification of Chemical Fibers and Polymer Materials, Donghua University, 2999 Renmin Rd. North, Songjiang District, Shanghai 201620, P.R. China  
E-mail: crwang@dhu.edu.cn  
Prof. L. Sun, Dr. X. Wu, Y. Wang, S. Li  
Key Laboratory of MEMS of Ministry of Education and School of Electronic Science and Engineering, Southeast University, Si-Pai-Lou 2, Nanjing 210096, P.R. China  
E-mail: slt@seu.edu.cn  
Prof. X. Chen, Prof. J. Chu  
National Laboratory for Infrared Physics, Shanghai Institute of Technical Physics, Chinese Academy of Science, Shanghai 200083, P.R. China  
E-mail: xschen@mail.sitp.ac.cn  
Prof. G.-C. Yi, H. Oh, H. Baek  
Department of Physics and Astronomy, Seoul National University, 599 Gwanak-ro, Gwanak-gu, Seoul 151-747, Korea  
E-mail: gychul.yi@gmail.com

[\*\*] This work was supported by the National Natural Science Foundation of China under Grant No. 11174049, 61376017, 11204030, 51071044, the Fundamental Research Funds for the Central Universities, the NSFC-NRF Scientific Cooperation Program, the National Research Foundation of Korea (NRF) Grant (NRF-2012K1A2B1A03000327), the Research Funds from Ministry of Education, China, the Natural Science Foundation of Jiangsu Province (No. BK2012024), and Chinese postdoctoral funding (No. 2012M520053).

### 1. Introduction

One-dimensional (1D) nanostructures have become the focus of intensive research owing to their unique thermal, mechanical, electron transport, phonon-transport, optical, and field-emission properties.<sup>[1]</sup> Especially 1D semiconductor nanowires, which have tremendous impacts on the development of modern science and technology, have been a hotspot. ZnSe (bulk crystal  $E_g = 2.7$  eV at 300 K),<sup>[2]</sup> as one of the key semiconductor materials for applications such as green laser diodes,<sup>[3]</sup> photodetectors,<sup>[4]</sup> field effect transistors (FETs),<sup>[5]</sup> and solar cells<sup>[6]</sup> has been widely investigated in recent years. ZnSe nanowires can be prepared by various methods, such as thermal evaporation,<sup>[6b]</sup> solution-based,<sup>[7]</sup> pulsed laser deposition,<sup>[8]</sup> and so on. Among them, thermal evaporation method based on vapor–liquid–solid (VLS)<sup>[9]</sup> growth mechanism has been generally employed,<sup>[2,6b,10]</sup> because the nucleation sites, structures, compositions, and sizes of 1D nanostructures can be well controlled by preformed metal catalysts.<sup>[11]</sup> Moreover, the nanostructures grown by the VLS growth mechanism often appears to be different in many experiments for multiple different growth modes,<sup>[12]</sup> which was even proved theoretically by the VLS growth of a hexagonal crystal in two dimensions for a single set of experimental conditions.<sup>[13]</sup>

During the growth of ZnSe nanowires, various defects such as point defects, stacking faults, and twinning defects, are formed, indicated in the related emission in photoluminescence spectra.<sup>[14]</sup> Among them, twinning is a kind of important defects in nanowires, as it could affect the migration of atoms and electrons in polycrystalline solids, thus influencing optical, electronic, and mechanical properties of the materials,<sup>[15]</sup> such as interrupting dislocation glide,<sup>[16]</sup> and strengthening the

material<sup>[17]</sup> without loss in electronic conductance.<sup>[16,18]</sup> Therefore, twinning, if suitably controlled, could add a new dimension in nanostructure device design.<sup>[19]</sup> Up to now, there are mainly two types of twinning nanowires reported: transverse twinning,<sup>[20]</sup> and longitudinal twinning,<sup>[21]</sup> in which, the twin plane is vertical and parallel to the axis of the nanowire, respectively. Transverse twinning nanowires, especially periodical or quasi-periodical twinning ZnSe nanowires have been investigated extensively.<sup>[2,22]</sup> However, the discontinuous electron wavefunctions at stacking faults might lead to smaller mobility of charge carriers<sup>[20a]</sup> of transverse twinning nanowires than that of the longitudinal twinning nanowires. Thus, introducing the longitudinal twinning into nanowire through a reasonable design is a perfect methodology to tailor the properties of nanowires. Allowing for ZnSe, two phases, wurtzite (WZ) and zinc blende (ZB), exist, and the (001) faces of WZ phase are indistinguishable from and can match up with the (111) faces of ZB phase,<sup>[23]</sup> the subtle structural differences of which lead to the attendant small difference in the internal energies ( $\approx 5.3$  meV atom<sup>-1</sup> for ZnSe<sup>[24]</sup>). Therefore, it is conceivable to introduce the longitudinal twinning into ZnSe during the phase transformation process between ZB phase ZnSe and WZ phase ZnSe, and at the same time, by analyzing the twinning nanowire, the phase transformation process of ZB and WZ will be more clearly demonstrated.

In present work, by a simple thermal evaporation method, we designed and observed the phase transformation process from WZ ZnSe nanowire to ZB ZnSe nanowire by using the high resolution-transmission electron microscope (HRTEM), which can be explained by the periodic slip mechanism. During the slip, the twinning would occur spontaneously in the nanowire. Once the twinning process was completed in the nanowire, the longitudinal twinning ZB ZnSe nanowire (Type I) was obtained; otherwise, the sandwich-structural nanowire, with WZ ZnSe subnanowire inserting into the out layers of the ZB ZnSe longitudinal twinning subnanowires at the twin plane (Type II), would be formed. The HRTEM images of the two types of nanowires match well with the simulated atomic models of them. Interestingly, the room-temperature Raman and low-temperature (10 K) photoluminescence (PL) spectroscopy of ZnSe-based longitudinal twinning nanowires confirm the influences of twinning on them, while the current-voltage curve of individual longitudinal twinning ZnSe nanowire demonstrate that the existence of longitudinal twinning in the ZnSe nanowires had no influence on the electrical transport properties of the ZnSe nanowires.

## 2. Results and Discussion

### 2.1. Morphology and Phases of the As-Grown Products

After the synthesis, yellow products were grown on the silicon substrates. Figure 1a and

b show the FESEM images of the products under different magnifications. From the images, the nanowires, with diameters of several tens of nanometers along the growth orientation and lengths of several micrometers, were observed. The tops of the nanowires have spherical particles, demonstrating the growth of the nanowires might follow the VLS growth mechanism.<sup>[9]</sup> Figure 1c shows the XRD pattern of the as-synthesized products. The diffraction peaks can be indexed to ZB ( $a = 5.6688$  Å, JCPDS No. 37-1463) and WZ ( $a = 3.996$  Å,  $c = 6.55$  Å, JCPDS No. 15-0105) ZnSe, respectively. The strong peak near 69° belongs to the Si substrate.

### 2.2. Crystal Structural Analysis

There are two kinds of longitudinal twinning nanowire in the products, named as Type I and Type II.

#### 2.2.1. Type I: ZB ZnSe Longitudinal Twinning Nanowire

Figure 2a shows the TEM image under low magnification of the nanowire of Type I, from which, a distinct interface on the nanowire can be observed. The energy dispersive spectrometer (EDS) patterns of the two sides of the interface marked as 1 and 2 are presented in Figure 2b, which demonstrate that the main compositions of the two sides are Cu, C, Si, and ZnSe. The signal of C and Cu might come from the TEM copper grid, and the Si signal may come from the Si substrate.

In order to get a clear understanding of the structure relationship of the twinning nanowires, HRTEM image (Figure 2c) and SAED pattern (Figure 2d) of the nanowire are obtained. From Figure 2c, a longitudinal twinning nanowire, with symmetrical lattice fringes indexed as  $(\bar{1}11)$  plane and  $(\bar{1}11)_t$  plane (subscript t stands for the corresponding twinning) of ZB ZnSe, could be observed. The angle between  $(\bar{1}11)$  plane (and  $(\bar{1}11)_t$  plane) and the twin plane was measured to be 70.1° (and 70.9°), and the growth direction was calculated to be along  $\langle 211 \rangle$ . SAED pattern (Figure 2d) confirms the ZB ZnSe structure, which can be indexed as

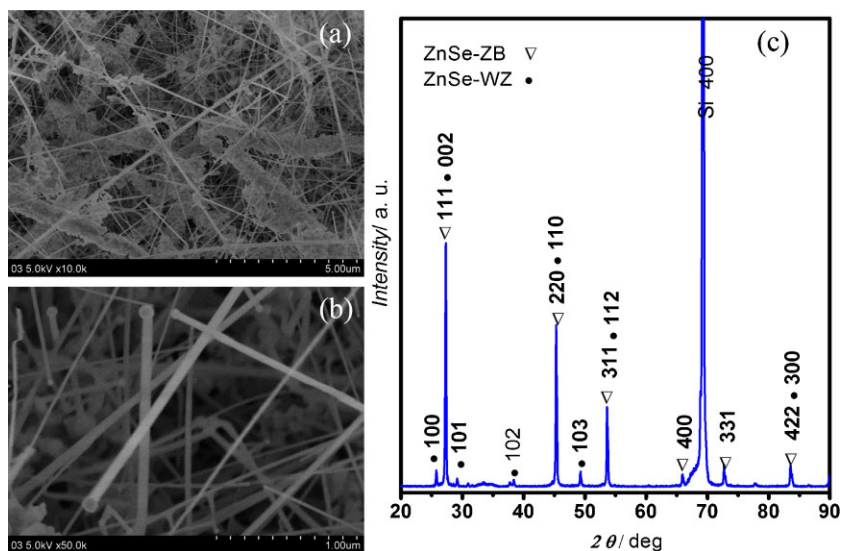


Fig. 1. FESEM images under different magnifications (a and b) and XRD pattern (c) of the products.

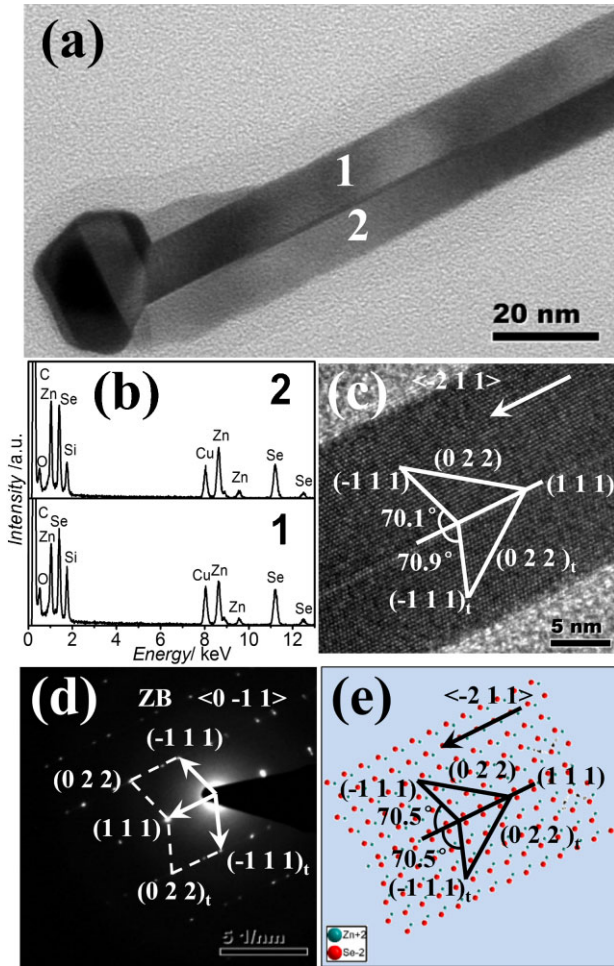


Fig. 2. (a) TEM image (scale bar: 20 nm), (b) EDS patterns of 1 and 2 in (a), (c) HRTEM image (scale bar: 5 nm), with (111) twin plane and growing along  $\langle 211 \rangle$ , (d) SAED pattern (scale bar: 5 nm), and (e) The simulated atomic model of the nanowire of Type I.

the  $\langle 0\bar{1}1 \rangle$  zone axis diffraction pattern, and the twin plane is (111). Figure 2e demonstrates the corresponding atomic model of the nanowire of Type I, projected along the  $\langle 0\bar{1}1 \rangle$  zone axis of ZB ZnSe, from which, the twin plane, the angle between  $(\bar{1}11)$  plane (and  $(\bar{1}11)_t$  plane) and the twin plane (111), and the growth direction confirm the results in Figure 2c and d.

### 2.2.2. Type II: Sandwich-Structural Longitudinal Twinning ZnSe Nanowires

Figure 3a shows the low magnification TEM image of the nanowire of Type II, from which, two distinct interfaces on the nanowire can be observed. The EDS patterns in Figure 3b indicate that the main compositions of the nanowire are Cu, C, Si, and ZnSe. The signal of C and Cu might come from the TEM grid, and the Si signal may come from the Si substrate.

From the HRTEM image in Figure 3c, the sandwich structural twinning nanowire can be clearly observed. The two outer subnanowires of the nanowire of Type II is symmetrical ZB ZnSe, with the twin plane of (111) and the growth direction of  $\langle 211 \rangle$ . The inner subnanowire of the nanowire is WZ ZnSe, growing along  $\langle 210 \rangle$  direction, inserting into the ZB ZnSe twinning nanowire along the twin boundary. From SAED pattern (Figure 3d), two sets of diffraction spots can be indexed as ZB  $\langle 0\bar{1}1 \rangle$  zone axis, and WZ  $\langle 010 \rangle$  zone axis of ZnSe, respectively, which confirms the symmetrical outer ZB ZnSe twinning subnanowires and the inner WZ ZnSe subnanowire. The atomic model of Type II is illustrated in Figure 3e, projected along the  $\langle 010 \rangle$  axis of WZ ZnSe and  $\langle 0\bar{1}1 \rangle$  axis of ZB ZnSe, which confirms the results of the HRTEM image in Figure 3c and the SAED pattern in Figure 3d.

However, the inner WZ ZnSe subnanowire in the atomic model seems to be a little different from that in the HRTEM image, i.e. there are (002) layers between every two adjacent (001) layers in the atomic model, while only (001) layers can be seen in the HRTEM image. This could be explained via the bottom-right inset of Figure 3e, which is the atomic model of the WZ ZnSe core projected along the growth direction  $\langle 210 \rangle$ . On the surface of the hexagonal ZnSe, Se atoms are suspended on the edges of the (001) layers, and there is no additional Se atoms hanging on the edges of (002) layers, which are in the middle of two adjacent (001) layers. That is the reason why the (002) plane cannot be seen in Figure 3c.

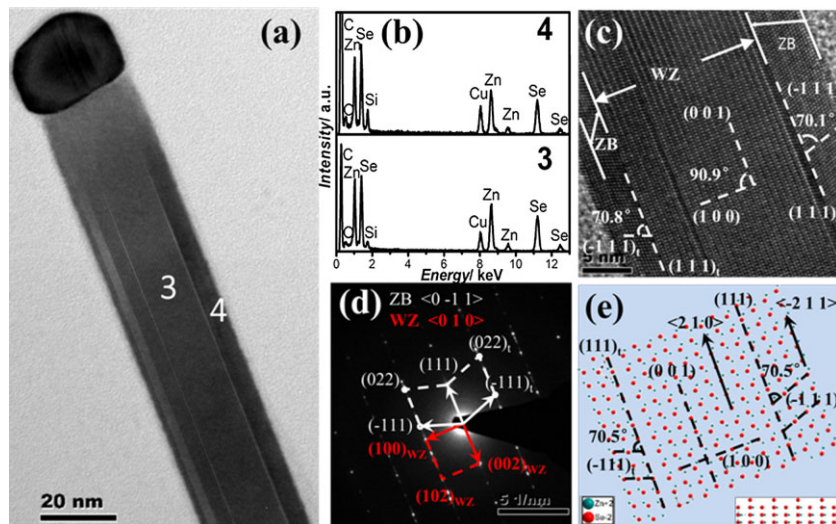


Fig. 3. (a) TEM image (scale bar: 20 nm), (b) EDS patterns of 3 and 4 in (a), (c) HRTEM image (scale bar: 5 nm), with WZ ZnSe core and ZB twinning ZnSe shell, (d) SAED pattern (scale bar: 5 nm), and (e) The simulated atomic model of the nanowire of Type II.

### 2.3. Possible Growth Mechanism of ZnSe-Based Longitudinal Twinning Nanowires

The as-grown longitudinal twinning nanowires in present work were considered to be caused by the crystal plane slip during the WZ–ZB phase transformation process. Structurally, the (001) planes of WZ and the (111) planes of ZB are their corresponding close packing planes. ABAB stacking for WZ and



and TO modes of ZnSe-based longitudinal twinning nanowire have 1–2  $\text{cm}^{-1}$  red-shift in comparison with those of the corresponding bulk counterpart ZnSe, which might be caused by the stacking faults<sup>[34]</sup> or the internal stresses<sup>[35]</sup> in the products.

Interestingly, the 2TA(X), LA(X), and defect related mode are absent in the Raman spectrum of defect-free ZnSe nanowires.<sup>[33,36]</sup> Generally speaking, Raman techniques is sensitive to the optical phonons close to the center of the Brillouin zone ( $q \approx 0$ ), the selection rule of which is essentially a consequence of the infinite periodicity of the crystal lattice. However, if the periodicity of the crystal is interrupted, as in the case of defects existing in the nanometer-sized materials, this rule is relaxed.<sup>[37]</sup>

### 2.5. Photoluminescence (PL)

Figure 6 shows the low-temperature PL spectrum (10 K) of the as-synthesized ZnSe-based longitudinal twinning nanowires. Two strong and broad emission peaks, centered at 1.974 and 2.329 eV, together with a series of sharp near-band-edge (NBE) emission peaks at high-energy region, were observed. The strongest red deep-level (DL) emission of 1.974 eV is confirmed due to a donor–acceptor-pair (DAP) recombination mechanism<sup>[38]</sup> or the self-activated-center (SA) luminescence<sup>[2,39]</sup> involving  $V_{\text{Zn}}$  as the acceptor species and  $V_{\text{Se}}$  or  $\text{Zn}_i$  as the donor species. The strong peak at 2.329 eV is usually attributed to the DL emission of unintentional incorporation of Cu<sup>[39]</sup> or Al,<sup>[2]</sup> but also sometimes attributed to an exciton at a  $V_{\text{Zn}}$  acceptor center.<sup>[39]</sup> In the present case, it should be attributed to Al impurity, because a trace amount of Al impurity (from the alumina substrate) may diffuse into the nanowire through surface diffusion during the growth of the products.<sup>[2]</sup>

The peaks at the high-energy region come from the NBE emission.<sup>[14,26a]</sup> The 2.769, 2.738, and 2.707 eV peaks are attributed to radiative recombination of an exciton bound to a neutral acceptor ( $A^0X$ ) with zero-phonon peak, the first phonon replica and second phonon replica of ZnSe, respec-

tively,<sup>[40]</sup> due to the LO-phonon ( $251 \text{ cm}^{-1}$ ) energy of ZnSe,  $\hbar\omega_{\text{LO}} = 31.4 \text{ meV}$ . It is notable that, a weak free exciton peak at around 2.826 eV can be observed, which consists of two peaks (2.829 and 2.822 eV) demonstrated in the inset of Figure 6. They are attributed to the upper polariton branch (UPB) and the lower polariton branch (LPB) of the resonant luminescence of free exciton–polaritons, respectively.<sup>[41]</sup> Using the energy of free exciton ( $E_g - E_X = 2.826 \text{ eV}$ ) and the bound exciton energy ( $h\nu = 2.769 \text{ eV}$ ), the dissociation energy of the exciton binding at the acceptor  $E_{\text{BX}} = E_g - E_X - h\nu = 57 \text{ meV}$ .

### 2.6. Electrical Properties

To study the electrical behavior of the twinning nanowires, the electrical measurements were carried out using a STM–TEM holder commercialized by Nanofactory Instruments AB, which is sketched in Figure 7a, as described in detail elsewhere.<sup>[42]</sup> A gold (Au) cantilever was attached to a fixed electrical sensor, whereas a platinum (Pt) cantilever placed on the piezo-movable side of the holder, was attached with the as-grown two types of nanowires (Figure 7b and c). The current–voltage ( $I$ – $V$ ) curves of them were plotted according to the  $I$ – $V$  data obtained when the voltage was ramped up, as shown in Figure 7e and f, which were recorded with a voltage ranging from  $-20$  to  $20 \text{ V}$  for  $1000 \text{ ms}$ . The two  $I$ – $V$  curves showed typically asymmetrical Schottky characteristic which might be caused by the lower work function of ZnSe than those of Pt and Au. By comparison, under the same conditions, the as-grown individual monocrystal ZnSe nanowire was also measured (Figure 7d). The obtained  $I$ – $V$  curve (Figure 7g) also showed asymmetrical Schottky characteristic and the current varied from  $-1.5$  to  $1.5 \text{ nA}$ , with no obvious differences from the curves obtained from the two types of twinning nanowires, which demonstrated that the existence of longitudinal twinning in the nanowires had no influence on the electrical transport properties of the nanowires. Moreover, the low current from the three ZnSe nanowires (Figure 7e–g) implied the high resistivity of ZnSe.

### 3. Conclusion

Two types of ZnSe-based longitudinal twinning nanowires, i.e. Type I) ZB longitudinal twinning ZnSe nanowires, and Type II) sandwich structures with WZ ZnSe subnanowires embedded between the two symmetrical outer ZB ZnSe longitudinal twinning nanowires, with diameters of several tens of nanometers along the growth orientation and lengths of several micrometers, were obtained through a simple thermal evaporation. The HRTEM images of the two kinds of longitudinal twinning nanowires match well with the simulated atomic models of them. The formation of them could be explained by the periodic slip mechanism during the WZ–ZB phase transformation process of ZnSe nanowires. In the room-temperature Raman spectra, the LA(X) phonon can be observed in the single ZnSe-based longitudinal nanowire, except for the commonly observed TO, LO, and 2TA(X) modes in the ZnSe-based longitudinal nanowires. From the low-

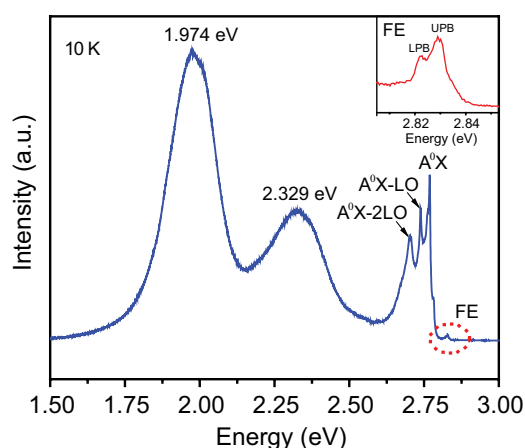


Fig. 6. Low-temperature (10 K) PL spectrum of ZnSe-based longitudinal twinning nanowires.

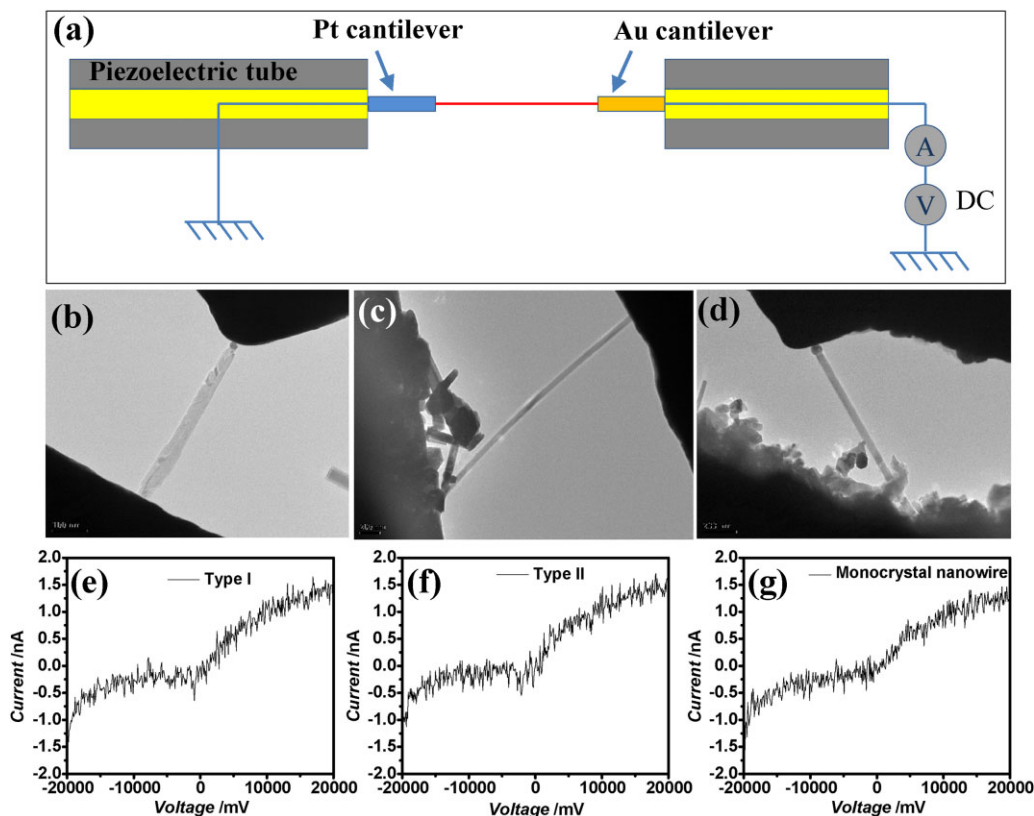


Fig. 7. (a) Schematic of the experimental set-up within a STM-TEM holder; (b)–(d) TEM views of individual Type I, Type II, and monocrystal ZnSe nanowires, respectively (Scale bars: 100 nm; 200 nm; 200 nm); (e)–(g) the corresponding current–voltage (I–V) curves of individual Type I, Type II, and monocrystal ZnSe nanowires, respectively.

temperature PL spectroscopy, two strong and broad emission peaks caused by DL emission, together with a series of sharp NBE emission peaks and a weak peak of free exciton at high-energy region, were observed. The existence of longitudinal twinning in the ZnSe nanowires had no influence on the electrical transport properties of the ZnSe nanowires. This quantitative study on the ZnSe-based longitudinal twinning nanowire’s structure, morphology, formation mechanism, electrical and optical behavior lends strong support to the feasibility of future 1D nanostructure fabrication, paving way for high performance optoelectronic devices.

#### 4. Experimental Section

ZnSe-based longitudinal twinning nanowires were synthesized by a high-temperature vacuum-tube furnace, which were described in detail elsewhere.<sup>[43]</sup> Briefly, the commercial ZnSe (99.99%, Alfa Aesar) powder was placed on alumina boats in the central region of the alumina tube. While silicon substrates, covered with chloroauric acid hydrated dissolved in the ethyl alcohol, were placed in downstream 12–22 cm from the furnace center to collect the products in the alumina tube. The furnace was then pumped down to a base pressure of  $\approx 1.2 \times 10^2$  Pa. Argon gas was introduced into the tube at a constant flow rate of 50 sccm (standard-state cubic centimeter per minute). The total pressure was kept at  $\approx 2.3 \times 10^2$  Pa during the experiment

process. The furnace was maintained at 1250 °C for 2 h before it cooled down to room temperature naturally.

The as-products were characterized by X-ray powder diffraction (XRD; Rigaku D/Max-2550), field emission scanning electron microscopy (FESEM; Hitachi S-4800), high-resolution transmission electron microscopy (HRTEM; TECHAI G<sup>2</sup> S-TWIN) equipped with an EDS. The Raman spectra were recorded on at room temperature in Via-Reflex micro-Raman spectroscopy system from Renishaw with 532 nm radiations. PL spectroscopy was performed at low temperature (10 K) using the 325 nm line of the He–Cd laser, as described elsewhere.<sup>[10]</sup> The electrical measurements were carried out using a new scanning tunnel microscope–transmission electron microscope (STM-TEM) holder commercialized by Nanofactory Instruments AB, which was arranged within a 200 kV field emission high-resolution TEM (HRTEM; JEM-2010F, JEOL Ltd., Tokyo, Japan).

Received: August 13, 2013

Final Version: November 18, 2013

Published online: January 20, 2014

- [1] Y. Xia, P. Yang, Y. Sun, Y. Wu, B. Mayers, B. Gates, Y. Yin, F. Kim, H. Yan, *Adv. Mater.* **2003**, *15*, 353.
- [2] Q. Li, X. G. Gong, C. R. Wang, J. Wang, K. Ip, S. Hark, *Adv. Mater.* **2004**, *16*, 1436.

- [3] A. A. Shakhmin, I. V. Sedova, S. V. Sorokin, M. V. Zamoryanskaya, *Phys. Status Solidi C* **2012**, *9*, 1840.
- [4] X. Fang, S. Xiong, T. Zhai, Y. Bando, M. Liao, U. K. Gautam, Y. Koide, X. Zhang, Y. Qian, D. Golberg, *Adv. Mater.* **2009**, *21*, 5016.
- [5] Q. Su, L. J. Li, S. Y. Li, H. P. Zhao, *Mater. Lett.* **2013**, *92*, 338.
- [6] a) Y. Zhang, Z. Wu, J. Zheng, X. Lin, H. Zhan, S. Li, J. Kang, J. Bleuse, H. Mariette, *Sol. Energ. Mat. Sol. C.* **2012**, *102*, 15; b) X. Zhang, X. Zhang, X. Zhang, Y. Zhang, L. Bian, Y. Wu, C. Xie, Y. Han, Y. Wang, P. Gao, L. Wang, J. Jie, *J. Mater. Chem.* **2012**, *22*, 22873.
- [7] H. Wei, Y. J. Su, S. Z. Chen, Y. Liu, Y. Lin, Y. F. Zhang, *Mater. Lett.* **2012**, *67*, 269.
- [8] J. S. Lai, L. Chen, X. N. Fu, J. Sun, Z. F. Ying, J. D. Wu, N. Xu, *Appl. Phys. A-mater.* **2011**, *102*, 477.
- [9] R. S. Wagner, W. C. Ellis, *Appl. Phys. Lett.* **1964**, *4*, 89.
- [10] C. R. Wang, J. Wang, Q. Li, G. C. Yi, *Adv. Funct. Mater.* **2005**, *15*, 1471.
- [11] a) S. K. Lim, S. Crawford, G. Haberfehlner, S. Gradecak, *Nano Lett.* **2013**, *13*, 331; b) R. E. Algra, M. A. Verheijen, L. F. Feiner, G. G. Immink, W. J. Enkevort, E. Vlieg, E. P. Bakkers, *Nano Lett.* **2011**, *11*, 1259; c) S. Crawford, S. K. Lim, S. Gradecak, *Nano Lett.* **2013**, *13*, 226.
- [12] a) V. Schmidt, S. Senz, U. Gösele, *Nano Lett.* **2005**, *5*, 931; b) H. Jagannathan, M. Deal, Y. Nishi, J. Woodruff, C. Chidsey, P. C. McIntyre, *J. Appl. Phys.* **2006**, *100*, 024318; c) P. Madras, E. Dailey, J. Drucker, *Nano Lett.* **2009**, *9*, 3826.
- [13] K. W. Schwarz, J. Tersoff, *Nano Lett.* **2012**, *12*, 1329.
- [14] U. Philipose, A. Saxena, H. E. Ruda, P. J. Simpson, Y. Q. Wang, K. L. Kavanagh, *Nanotechnology* **2008**, *19*, 215715.
- [15] a) K.-C. Chen, W.-W. Wu, C.-N. Liao, L.-J. Chen, K. Tu, *Science* **2008**, *321*, 1066; b) Z. Ikončić, G. Srivastava, J. Inkson, *Phys. Rev. B* **1993**, *48*, 17181; c) Z. Ikončić, G. Srivastava, J. Inkson, *Phys. Rev. B* **1995**, *52*, 14078.
- [16] L. Lu, Y. Shen, X. Chen, L. Qian, K. Lu, *Science* **2004**, *304*, 422.
- [17] B. Wu, A. Heidelberg, J. J. Boland, J. E. Sader, Sun, Li, *Nano Lett.* **2006**, *6*, 468.
- [18] a) Y. Zhang, H. Huang, *J. Appl. Phys.* **2010**, *108*, 103507; b) S. Zhong, T. Koch, M. Wang, T. Scherer, S. Walheim, H. Hahn, T. Schimmel, *Small* **2009**, *5*, 2265.
- [19] J. Bao, D. C. Bell, F. Capasso, J. B. Wagner, T. M. rtensson, J. Träg rdh, L. Samuelson, *Nano Lett.* **2008**, *8*, 836.
- [20] a) R. E. Algra, M. A. Verheijen, M. T. Borgstrom, L. F. Feiner, G. Immink, W. J. van Enkevort, E. Vlieg, E. P. Bakkers, *Nature* **2008**, *456*, 369; b) Y. Hao, G. Meng, Z. L. Wang, C. Ye, L. Zhang, *Nano Lett.* **2006**, *6*, 1650.
- [21] a) Y. Dai, Y. Zhang, Y. Q. Bai, Z. L. Wang, *Chem. Phys. Lett.* **2003**, *375*, 96; b) Y. Ding, Z. L. Wang, *J. Phys. Chem. B* **2004**, *108*, 12280.
- [22] a) Y. Q. Wang, U. Philipose, T. Xu, H. E. Ruda, K. L. Kavanagh, *Semicond. Sci. Technol.* **2007**, *22*, 175; b) X. Fan, X. M. Meng, X. H. Zhang, M. L. Zhang, J. S. Jie, W. J. Zhang, C. S. Lee, S. T. Lee, *J. Phys. Chem. C* **2008**, *113*, 834.
- [23] S. M. Hughes, A. P. Alivisatos, *Nano Lett.* **2013**, *13*, 106.
- [24] C.-Y. Yeh, Z. Lu, S. Froyen, A. Zunger, *Phys. Rev. B* **1992**, *46*, 10086.
- [25] P. Williams, A. Yoffe, *Philos. Mag.* **1972**, *25*, 247.
- [26] a) L. Jin, W. C. H. Choy, Y. P. Leung, T. I. Yuk, H. C. Ong, J. B. Wang, *J. Appl. Phys.* **2007**, *102*, 044302; b) H. Okada, T. Kawanaka, S. Ohmoto, *J. Cryst. Growth* **1996**, *165*, 31.
- [27] a) S. Li, G. W. Yang, *J. Phys. Chem. C* **2010**, *114*, 15054; b) S. Qadri, E. Skelton, D. Hsu, A. Dinsmore, J. Yang, H. Gray, B. Ratna, *Phys. Rev. B* **1999**, *60*, 9191.
- [28] Y. Ding, X. D. Wang, Z. L. Wang, *Chem. Phys. Lett.* **2004**, *398*, 32.
- [29] M. J. Scepanovic, M. Grujic-Brojcin, I. Bineva, D. Nesheva, Z. Aneva, Z. Levi, Z. V. Popovic, *J. Optoelectron. Adv. M* **2007**, *9*, 178.
- [30] Y. Jiang, X. M. Meng, W. C. Yiu, J. Liu, J. X. Ding, C. S. Lee, S. T. Lee, *J. Phys. Chem. B* **2004**, *108*, 2784.
- [31] a) G. W. Lu, H. Z. An, Y. Chen, J. H. Huang, H. Z. Zhang, B. Xiang, Q. Zhao, D. P. Yu, W. M. Du, *J. Cryst. Growth* **2005**, *274*, 530; b) H-o. Yugami, S-i. Nakashima, K. Sakai, H. Kojima, M. Hangyo, A. Mitsuishi, *J. Phys. Soc. Jpn.* **1987**, *56*, 1881; c) A. Krost, W. Richter, D. Zahn, K. Hingerl, H. Sitter, *Appl. Phys. Lett.* **1990**, *57*, 1981; d) Y. Yu, J. Zhou, H. Han, C. Zhang, T. Cai, C. Song, T. Gao, *J. Alloy. Compd.* **2009**, *471*, 492.
- [32] F. Wang, Z. Zhang, R. Liu, X. Wang, X. Zhu, A. Pan, B. Zou, *Nanotechnology* **2007**, *18*, 305705.
- [33] C. X. Shan, Z. Liu, X. T. Zhang, C. C. Wong, S. K. Hark, *Nanotechnology* **2006**, *17*, 5561.
- [34] S.-L. Zhang, B.-F. Zhu, F. Huang, Y. Yan, E.-Y. Shang, S. Fan, W. Han, *Solid State Commun.* **1999**, *111*, 647.
- [35] H. Mukaida, H. Okumura, J. Lee, H. Daimon, E. Sakuma, S. Misawa, K. Endo, S. Yoshida, *J. Appl. Phys.* **1987**, *62*, 254.
- [36] X. F. Xu, C. R. Wang, J. A. Liu, J. S. Cai, X. S. Chen, *Chem. Phys. Lett.* **2011**, *501*, 491.
- [37] A. K. Arora, M. Rajalakshmi, T. Ravindran, V. Sivasubramanian, *J. Raman. Spectrosc.* **2007**, *38*, 604.
- [38] U. Philipose, S. Yang, T. Xu, H. E. Ruda, *Appl. Phys. Lett.* **2007**, *90*, 063103.
- [39] J. Gutowski, N. Presser, G. Kudlek, *Phys. Status. Solidi. A* **1990**, *120*, 11.
- [40] P. J. Dean, B. J. Fitzpatrick, R. N. Bhargava, *Phys. Rev. B* **1982**, *26*, 2016.
- [41] E. S. Koteles, J. Lee, J. P. Salerno, M. O. Vassell, *Phys. Rev. Lett.* **1985**, *55*, 867.
- [42] a) R. Zou, L. Yu, Z. Zhang, Z. Chen, J. Hu, *Nanoscale Res. Lett.* **2011**, *6*, 473; b) X. Liu, C. Wang, J. Xu, X. Liu, R. Zou, L. Ouyang, X. Xu, X. Chen, H. Xing, *CrystEngComm* **2013**, *15*, 1139.
- [43] J. Xu, C. R. Wang, Y. Zhang, X. Liu, X. Y. Liu, S. Y. Huang, X. S. Chen, *CrystEngComm* **2013**, *15*, 764.